ÓPTICA PURA Y APLICADA
www.sedoptica.es

Type: RESEARCH PAPER
Section: OPTICAL METROLOGY AND INSTRUMENTATION

Sign determination in temporal speckle pattern interferometry without using a temporal carrier

Determinación del signo en interferometría de patrones de speckle temporales sin utilizar una portadora temporal

Lucas P. Tendela[1,2*], Gustavo E. Galizzi[1,2]

1. Instituto de Física Rosario (CONICET – UNR), Blvd. 27 de Febrero 210 bis, S2000EZP, Rosario, Argentina.

2. Universidad Nacional de Rosario, Facultad de Ciencias Exactas, Ingeniería y Agrimensura, Av. Pellegrini 250, S2000BTP, Rosario, Argentina.

(*) E-mail: tendela@ifir-conicet.gov.ar

Received: 29/03/2023 Accepted: 16/06/2023
DOI: 10.7149/OPA.56.2.51141

ABSTRACT:

In this paper, we present a novel method to detect the correct sign of non-monotonous displacements in temporal speckle pattern interferometry without the introduction of a temporal carrier in the optical setup. The present work is based on a previous one, where the sign ambiguity is eliminated due to a function that determines the correct sign of the displacement between two consecutive speckle interferograms. Although that approach does not need the introduction of a phase-shifting facility or spatial carrier fringes in the optical setup, the intensities of the object and the reference beams must be recorded separately, which complicates the application of this method for the analysis of non-repeatable dynamic phenomena. Here, the proposed function can be applied when the displacement fields between the successive frames are in the nanometer range, and there is no need to acquire the intensities of the object and the reference beams. The performance of the proposed function and its limitations are determined using computer-simulated speckle interferograms. Finally, an experimental application of the proposed method is also illustrated.

Key words: Phase evaluation; Sign determination; Non-monotonous phase changes

RESUMEN: En este artículo, presentamos un método novedoso para detectar el signo correcto de desplazamientos no monótonos en la interferometría de patrones de speckle temporales sin la introducción de una portadora temporal en la configuración óptica. El presente trabajo se basa en uno anterior, donde se elimina la ambigüedad de signo gracias a una función que determina el signo correcto del desplazamiento entre dos interferogramas de speckle consecutivos. Aunque ese enfoque no necesita la introducción de un dispositivo de cambio de fase o franjas de portadores espaciales en la configuración óptica, las intensidades del objeto y los haces de referencia deben registrarse por separado, lo que complica la aplicación de este método para el análisis de fenómenos dinámicos no repetibles. Aquí, la función propuesta se puede aplicar cuando los campos de desplazamiento entre las imágenes sucesivas están en el rango de nanómetros, y no hay necesidad de adquirir las intensidades de los haces del objeto y de referencia. El rendimiento de la función propuesta y sus limitaciones se determinan utilizando interferogramas de speckle simulados por computadora. Finalmente, también se ilustra una aplicación experimental del método propuesto.

Palabras clave: Evaluación de fase; Determinación de signo; Cambios de fase no monótonos

REFERENCES AND LINKS / REFERENCIAS Y ENLACES

[1] P. K. Rastogi, *Digital speckle pattern interferometry and related techniques*, Chichester, John Wiley & Sons Ltd., (2001).

[2] G. H. Kaufmann, *Advances in speckle metrology and related techniques*, Weinheim, Wiley-VCH Verlag & Co., 147–205 (2011).

[3] W. Osten, *Optical Inspection of Microsystems*, 2nd ed., Taylor & Francis (2019).

[4] R. Kulkarni, P. K. Rastogi, "Optical measurement techniques – A push for digitization," Opt Lasers Eng 87, 1-17 (2016).

[5] P. Etchepareborda, A. Bianchetti, F. E. Veiras, A. L. Vadnjal, A. Federico, G. H. Kaufmann, "Comparison of real-time phase-reconstruction methods in temporal speckle-pattern interferometry," Appl Opt 54, 7663-7672 (2015).

[6] G. Rilling, P. Flandrin, P. Gonalves, J. Lilly, "Bivariate empirical mode decomposition," IEEE Signal Process. Lett. 14, 936–939 (2007).

[7] A. Eftekhar, C. Toumazou, E. M. Drakakis, "Empirical mode decomposition: Real-time implementation and applications," J. Signal Process. Syst. 73, 43–58 (2013).

[8] J. M. Huntley, *Automated analysis of speckle interferograms*, Chichester, John Wiley & Sons Ltd., 59–139 (2001).

[9] N. D. Borza, Ioana T. Nistea, "High temporal and spatial resolution in time resolved speckle interferometry," Opt Lasers Eng 50, 1075-1083 (2012).

[10] M. Takeda, H. Ina, S. Kobayashi, "Fourier Transform method of fringe analysis for computer-based topography and interferometry," J Opt Soc Am 72, 156–160 (1982).

[11] Q. Kemao, "Two-dimensional windowed Fourier transform for fringe pattern analysis: principles, applications and implementations," Opt Lasers Eng 45, 304-317 (2007).

[12] G.E. Galizzi, A. Federico, and G.H. Kaufmann, "Experimental evaluation of a 3D wavelet-based phase recovery 304 method in temporal speckle pattern interferometry," Appl Opt 56, 4412–4418 (2017).

[13] H. Pokharna, G. S. Schajer, ""Quasi Single-frame Measurements with Phase-stepped ESPI," Opt Lasers Eng 121, 181-188 (2019).

[14] Y. Du, H. Zhao, Z. Zhao, "Sign-singularity solution in single-frame speckle interferometry with vortex-phase modulation," Opt Lett 47, 2927-2930 (2022)."

[15] L.P. Tendela, G.E. Galizzi, A. Federico, G.H. Kaufmann, "Measurement of non-monotonous phase changes in temporal speckle pattern interferometry using a correlation method without a temporal carrier," Opt Lasers Eng **73**, 16-21 (2015).

[16] L.P. Tendela, and G.E. Galizzi, "Sign determination to measure non-monotonous displacements in temporal speckle pattern interferometry without a temporal carrier," Opt Lasers Eng **161**, 107353 (2023).

1. Introduction

As it is well-known, temporal speckle pattern interferometry (TSPI) is one of the most appropriate techniques for measuring dynamic displacement fields of optically rough objects (see Refs. [1–3] and references therein). Its main advantages include its high sensitivity and the possibility of real time, contactless and whole-field measurements with no surface preparation of the tested object [3]. Usually, the phase distribution can be obtained using different phase recovery techniques, and applying a phase unwrapping method along the temporal dimension. Until recently, to distinguish positive displacements from negative displacements, a known phase carrier was added to the phase function, which is linear in either time or position [1]. In both cases, the resulting phase distribution is a monotonic increasing or decreasing function.

On one hand, phase estimation in interferometric measurements commonly employs temporal phase shifting, which involves recording multiple phase-stepped intensity patterns [1, 4]. Various phase shifting algorithms have been proposed to achieve accurate phase estimation [5–7]. Great precision, noise robustness, great computational efficiency, and the capacity to work with low contrast fringe patterns are some of the major characteristics of phase shifting technology. The primary drawback of this method is that only static deformation measurements can be used with it. However, attempts have also been made to broaden the applicability of the approach to assess dynamic deformations [8, 9], relying on temporal phase unwrapping. On the other hand, by deliberately inserting a known linear phase into the interferometric system before the object deforms, carrier fringes are instead produced in the spatial methods of phase

estimation [1, 8]. These carrier fringes are modulated by the subsequent object deformation. To assess the phase associated with object deformation, the carrier fringe pattern demodulation based on Fourier transform [10], Windowed Fourier transform [11], and Wavelet transform [12] has been developed. Therefore, the main difference between the spatial and temporal methods of fringe processing is that while the former involves spatial carrier the latter involves temporal carrier to carry the phase information.

The experimental conditions do not always allow the application of phase shifting or addition of carrier fringes. To overcome this limitation, different phase-recovery approaches have been proposed such as the single-shot phase-stepped DSPI technique based on the image interpolation method [13], or the single-frame vortex-phase modulation [14].

Recently, Tendela et *al.* [15] have presented a phase retrieval approach based on a correlation method, that overcomes the sign ambiguity problem without a temporal carrier. More recently, Tendela et *al.* [16] proposed a generalized function to automatically detect the correct sign of the displacement to be used in a TSPI system for *any* phase retrieval approach. Although these approaches do not need the introduction of a phase-shifting facility or spatial carrier fringes in the optical setup, the intensities of the object and the reference beams must be recorded separately. It should be noted that this limitation complicates the automation of the interferometer operation.

To overcome the above-mentioned limitation, in this paper we propose a novel function based on the Tendela method reported in Ref. [16], when the displacement fields are in the nanometer range. The proposed function does not need to record separately the intensities of the object and the reference beams. It is worthwhile to mention that cases of phase distribution patterns presenting small phase changes can appear quite frequently when microsystems are inspected [3]. The errors introduced by the proposed function and its limitations are determined using computer-simulated speckle interferograms. Finally, an application of the proposed function to detect the correct sign of the out-of-plane displacement field of a metal plate is also illustrated.

2. Theoretical concepts

TSPI basically involves the interference of two optical waves, of which at least one represents a speckle wave. In these cases, the intensity distribution $I(x,y,t)$ recorded by the CCD camera, without introducing a temporal carrier in the interferometer, is given by [1]

$$I(x,y,t) = I_0(x,y,t) + I_M(x,y,t)\ \cos\big(\phi(x,y,t)\big), \tag{1}$$

where $I_0(x,y,t)$ is the background intensity, $I_M(x,y,t)$ is the modulation intensity, $\phi(x,y,t)$ is the phase to be measured, x = 1, 2, ..., n_x and y = 1 ,2, ..., n_y are the spatial coordinates of the camera pixels and t = 1, ..., n_t is the temporal coordinate or frame number.

As explained in Ref. [16], the phase ϕ at a frame t_i can be computed as

$$\phi(t_i) = \sum_{j=1}^{t_i} S\big(t_{j-1}, t_j\big)\ \ \Delta\phi\big(t_{j-1}, t_j\big), \tag{2}$$

where $S(t_{i-1},\ t_i)$ is the function that determines the correct sign of the displacement and $\Delta\phi(t_{i-1},t_i)$ corresponds to the deterministic phase change introduced by the underwent deformation, between the successive frames t_{i-1} and t_i. It is important to mention that $\Delta\phi(t_{i-1},\ t_i)$ is always in the range $[0,\pi]$ rad, so the temporal phase is properly sampled. The sign function $S(t_{i-1},\ t_i)$, that determines the correct sign of the displacement between the successive frames t_{i-1} and t_i, is defined as [16]

$$S(t_{i-1}, t_i) = \text{sign}\{\phi(t_{i-1})\} \times \text{sign}\{I_0 + [I(t_{i-1}) - I_0]\cos[\Delta\phi(t_{i-1}, t_i)] - I(t_i)\}, \tag{3}$$

where the x and y spatial coordinates were omitted for the sake of clarity. It is worthwhile to mention that the deterministic phase distribution $\Delta\phi(t_{i-1},\ t_i)$ can be evaluated by means of *any* phase retrieval approach.

In addition, the background bias I_0 is defined as I_0=I_1 + I_2, where I_1 and I_2 are the intensities of the object and the reference optical fields. Therefore, in order to compute I_0 it is necessary to record separately the

intensities of the object and the reference beams at any time of the experiment [16]. In some cases, this procedure might complicate the automation of the interferometer operation. In addition, this limitation does not allow the application of this method reported in Ref. [16] for the analysis of non-repeatable dynamic events.

Here, we present an approximation that overcomes this limitation when the phase changes between two successive frames are small, i.e., when $\cos[\Delta\phi(t_{i-1}, t_i)] \approx 1$. Considering this relation, $S(t_{i-1}, t_i)$ in Eq. (3) can be approximated as

$$S(t_{i-1}, t_i) \approx S_A(t_{i-1}, t_i) = \text{sign}\{\phi(t_{i-1})\} \times \text{sign}\{I(t_{i-1}) - I(t_i)\}, \quad (4)$$

where S_A is the approximation of the sign function.

Furthermore, when the first frame t=1 is considered, the random phase change $\phi(0)=\phi_s$ due to the roughness of the scattering surface must be determined. In the cases where the proposed method can be applied, the phase changes of the first four successive frames of the image sequence are small and can be considered approximately equal. Therefore, a multiple-frame phase-calculation method, such as the Carré technique, can be used to determine ϕ_s.

Although in this section it was shown that the correct sign of the displacement can be determined pixel by pixel, the accuracy of the functions S and S_A strongly depends on the average speckle sizes d_{sp} [16]. The functions S and S_A must be computed inside a sliding window of side $W_s \times W_s$ pixels, where W_s has to be larger than d_{sp}. The reader can find more details of how to determine the correct sign of the phase change in Ref. [16].

3. Numerical results

The speckle interferograms used to evaluate the performance of the proposed function S_A were generated by computer simulation, using the same approach to the one applied in Ref. [16]. As the input phase distribution produced by a sequence of computer-simulated speckle interferograms is known precisely, this approach allows us to determine the errors introduced by the algorithm used for determining the correct sign. Furthermore, the simulated speckle distributions were generated with a resolution of n_x=n_y=512 pixels, and each data set contained n_t=512 images. The average speckle size was set as d_{sp}=2 pixels. In all cases, the phase distributions were recovered by means of the Fourier transform technique (1DFFT) [10].

Firstly, the input phase distribution simulates a spherical cap that inflates until the frame 256, and then deflates (see Fig. 1). The temporal evolution of the retrieved phase distribution evaluated with the 1DFFT method (bold curve) and the original input phase map (solid circles) for the central pixel of the pattern are shown in Fig. 2. The low and high cut-off frequencies using the 1DFFT method were F_L = 25 and F_H = 125, respectively. In this example, the sign was determined using a sliding window of $W_s^2 = 64 \times 64$ pixels. From this last figure, it can be seen that there is a good agreement between the original phase changes and the phase values obtained using the 1DFFT method combined with the function S_A. It is important to note that, as shown in Ref. [16], the performance of the original method to determine the correct sign (i.e., by means of Eq. (3)) strongly depends on the retrieved phase techniques used. Therefore, it is to be expected that the same will happen with the simplified approach (i.e., by means of Eq. (4)). In this example, the percentage of pixels that weren't determined with their correct signs is 0.003%. That is, the proposed method only failed to recover the correct sign of the phase in 3544 pixels out of the total number of pixels analysed $N_T = (n_x - W_s) \times (n_y - W_s) \times n_t \approx 100.000.000$.

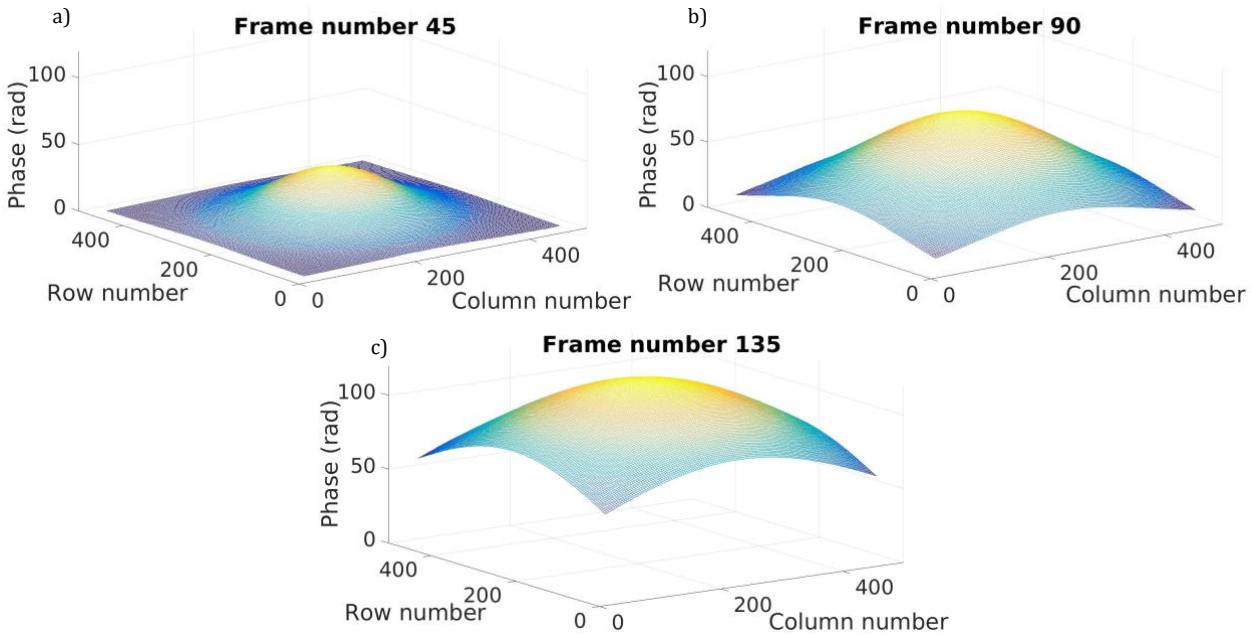

Fig.1. Temporal evolution of the phase evaluated using the 1DFFT method corresponding to the inflate stage, (a) frame number 45, (b) frame number 90, and (c) frame number 135.

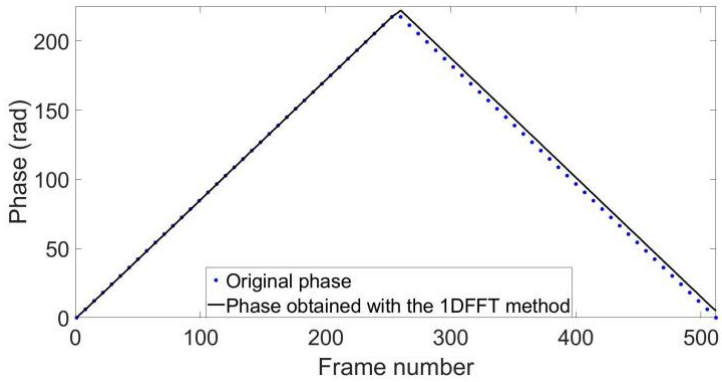

Fig.2. Comparison between the temporal evolution of the original phase (solid circles) and the phase obtained with the 1DFFT method (bold curve), for the central pixel of the pattern corresponding to the same displacement shown in Fig. 1. The function S_A was computed using a sliding window of size W_s^2=64×64 pixels.

Secondly, an in-plane linear increasing and decreasing phase change of 0.25 rad per frame was simulated. Figure 3 depicts the phase distributions evaluated with the 1DFFT method (bold curve) and the original input phase map (solid circles). It is important to mention that the function S_A was computed using a sliding window of W_s^2 = 20×20 pixels. In this simulation, the low and high cut-off frequencies using the 1DFFT method were F_L=5 and F_H=150, respectively. From this last figure, it can be seen that there is a good agreement between the original phase changes and obtained using the 1DFFT method combined with the function S_A. In this second example, the percentage of pixels that weren't determined with their correct signs is 0.002%.

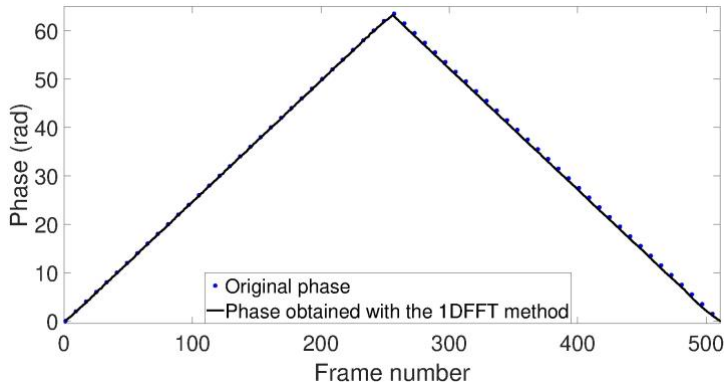

Fig.3. Comparison between the temporal evolution of the original phase (solid circles) and the phase obtained with the 1DFFT method (bold curve), for the central pixel of the pattern corresponding to a simulated in-plane linear non-monotonous displacement. The function S_A was computed using a sliding window of size W_s^2=20×20 pixels.

It is necessary to point out that in the previous simulations, the value of cos $\Delta\phi$ was approximately 1 to ensure the validity of Eq. (4).

To test the limit of the validity of Eq. (4), a new simulation was performed. Figure 4 shows the plot of the temporal evolution of the retrieved phase distribution using the function S_A and evaluated with the 1DFFT method (bold curve), when the out-of-plane non-monotonous phase is given by $f(t)$=0.5 t/n_t sin(π t/n_t) (solid circles). In this case, the low and high cut-off frequencies using the 1DFFT method were F_L=2 and F_H=200, respectively. This figure also depicts cos $\Delta\phi$ (dashed line) in order to verify the limits of the proposed method. From Fig. 4, it can be seen that the phase distribution is recovered properly until the frame 365, where cos $\Delta\phi \approx 0.6$. It should be noted that after this frame, the phase changes between two consecutive frames are large enough for the cosine approximation to fail.

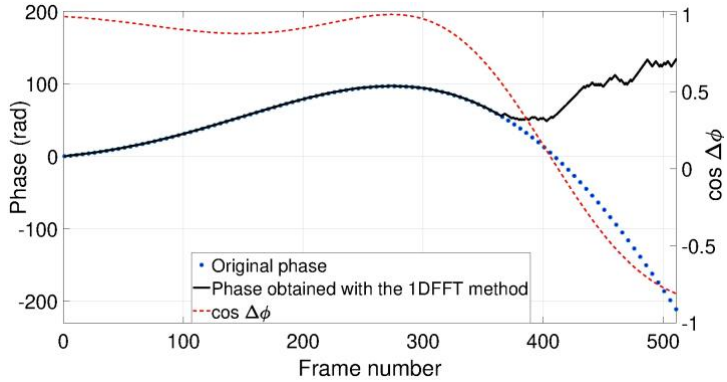

Fig.4. Comparison between the temporal evolution of the original phase (solid circles) and the phase obtained using the 1DFFT method (bold curve), for the central pixel of the pattern corresponding to a simulated out-of-plane non-monotonous phase change. The function S_A was computed using a sliding window of size W_s^2 = 14×14 pixels. The same figure also shows cos $\Delta\phi$ (dashed line).

Finally, Fig. 5 shows that the 1DFFT method determines the correct sign of the displacement field until the frame 365 approximately, corresponding to the same measurement depicted in Fig. 4. From Figs. 4 and 5, it can be seen that there is a good agreement between the original phase changes and obtained using the 1DFFT method combined with the function S_A until the frame 365. Therefore, the approximation in Eq. (3) could be considered valid when cos $\Delta\phi > 0.6$.

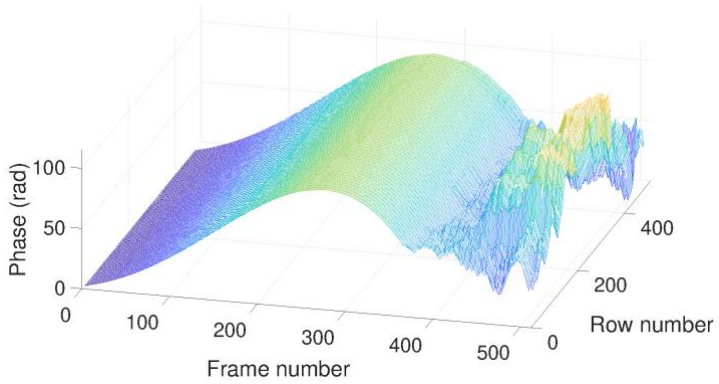

Fig.5. Temporal evolution of the phase evaluated using the 1DFFT method for pixels in the central column of the image, corresponding to the same measurement shown in Fig. 2.

4. Experimental Results

The performance of the function S_A was experimentally analyzed using the same datasets as in Ref. [16]. Here, a conventional speckle interferometer with out-of-plane sensitivity was used to measure the phase changes generated by a specimen attached to a nanopositioner stage. The specimen was an aluminium plate attached to a nanopositioner Physik Instrumente P-611.Z Z Stage (PZT). A Physik Instrumente E-625 Servo-Controller acted as the control unit (CU) that applies a voltage to the nanopositioner. The applied voltage generates a rigid body displacement of the specimen, which is the same for every point of the object surface.

The CU was programmed to displace linearly moving the specimen closer and farther from the CCD camera, which generates a constant temporal variation in the phase of nearly $\pi/5$ rad between successive frames (*i.e.*, $\cos(\pi/5) \approx 0.8$). In this experiment, the low and high cut-off frequencies using the 1DFFT method were F_L=30 and F_H=200, respectively.

Figure 6 depicts the temporal evolution of the phase evaluated for the central pixel of the image using the function S_A and evaluated with the 1DFFT method (bold line). The function S_A was computed for each method using a sliding window of size $W_s^2 = 64 \times 64$ pixels. The same figure also shows the programmed phase (solid circles), which corresponds to the phase produced with the displacement generated by PZT. It can be noticed that there is a good agreement between the evaluated phase values using the 1DFFT method and the programmed phase.

To show that the phase distribution is recovered with its correct sign, Fig. 7 depicts the voltage difference applied to PZT between the successive frames (in dash line and with arbitrary units), and the function S_A (bold line) for the central pixel of the image. Therefore, the change in the sign corresponds to a change in the applied voltage difference, meaning that the direction of the displacement had changed.

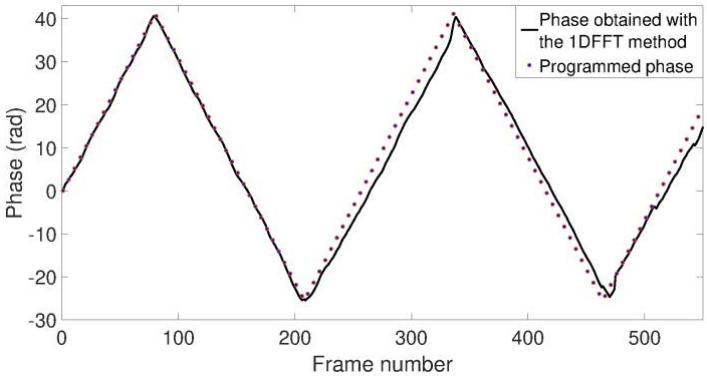

Fig.6. Temporal evolution of the phase obtained with the 1DFFT method (bold line) for the central pixel of the image, and the programmed phase (solid circles). The function S_A was computed for each method using a sliding window of size $W_s^2 = 64 \times 64$ pixels.

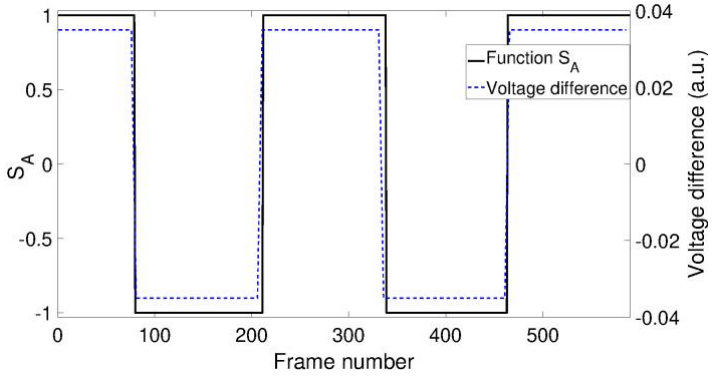

Fig.7. Temporal evolution of the function S_A (bold line) for the central pixel of the image, and voltage difference applied to PZT between successive frames (dash line and arbitrary units).

Finally, Fig. 8, shows that the recovered phase obtained with the 1DFFT method is similar for the pixels located along the central column of the image, and no errors were introduced due to the function S_A. Furthermore, it can be noticed that the noise in the retrieved phase depends on the method used to obtain the phase distribution [16].

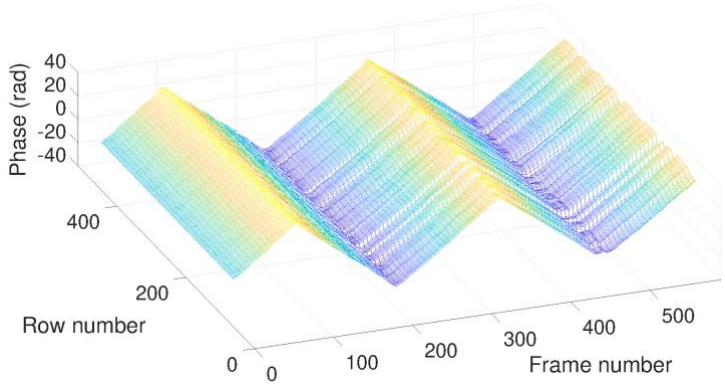

Fig.8. Temporal evolution of the phase evaluated using the 1DFFT method for pixels in the central column of the image, corresponding to the same measurement shown in Fig. 4. The function S_A was computed using a sliding window of size $W_s^2 = 64 \times 64$ pixels.

4. Conclusions

In this paper we propose a novel approach to automatically detect the correct sign of non-monotonous displacements in temporal speckle pattern interferometry without the introduction of a temporal carrier in the optical setup. In this method there is no need to record the intensities of the object and the reference beams. Therefore, the main highlight of this technique is that the sign ambiguity is resolved automatically due to the introduction of a function that determines the correct sign of the displacement between two consecutive speckle interferograms. This advantage not only makes easier the automation of the interferometer operation, but also allows the application of the proposed method to the analysis of non-repeatable dynamic events by recording a sequence of interferograms throughout the entire deformation history of the testing object.

It is well-known that the performance of phase retrieval methods used in TSPI depends on various parameters, such as the sensitivity vector direction of the interferometer (for in-plane or out-of-plane displacement measurements), average speckle size, filter sizes used in each phase retrieval method, window sizes, and more. The difference in performance lies in the method used to retrieve the signless phase. If the technique employed for signless phase recovery has poor performance, the proposed method for determining the sign will yield unsatisfactory results. By using different computer-simulated phase change distributions, the proposed method demonstrates acceptable performance, with a relatively small number of pixels failing to recover the correct sign out of the total analyzed. Finally, these results given by the numerical analysis are confirmed by processing experimental data obtained from the analysis of an aluminium plate when it is attached to a nanopositioner that was programmed to displace linearly moving closer and farther from the CCD camera.

Acknowledgements

The authors wish to thank the financial support of CONICET (PIP11220150100607) and Universidad Nacional de Rosario (80020190300107UR).

